Supplementary Figure 1

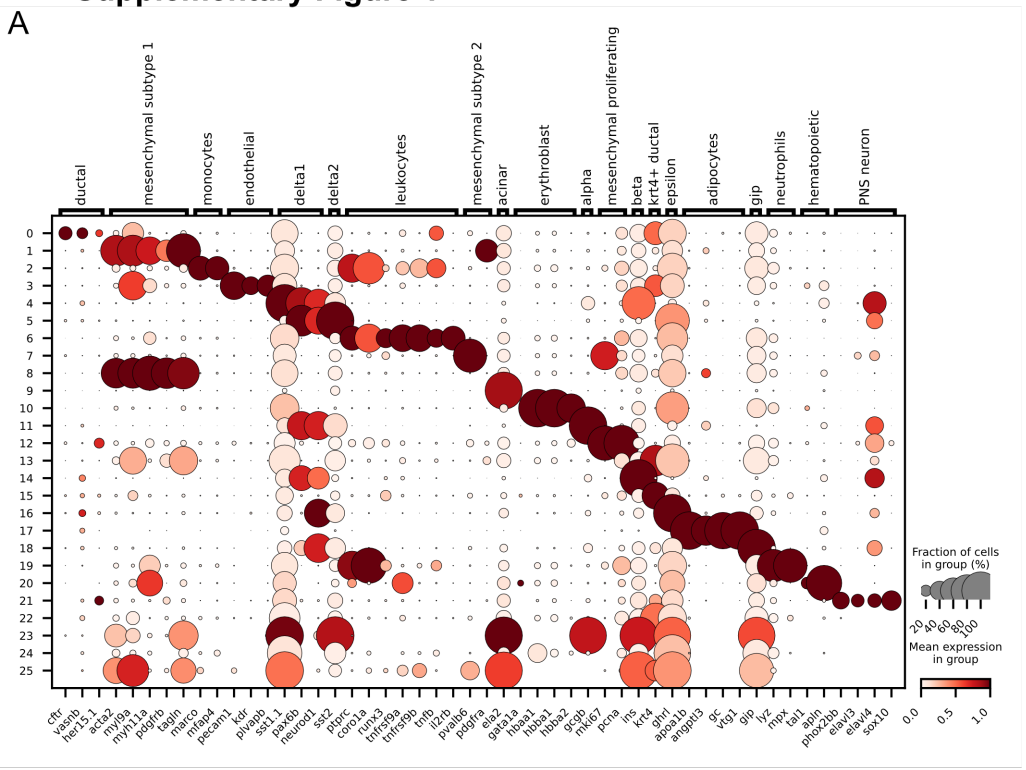

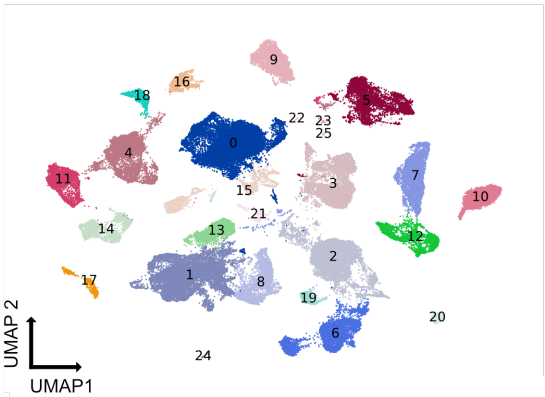

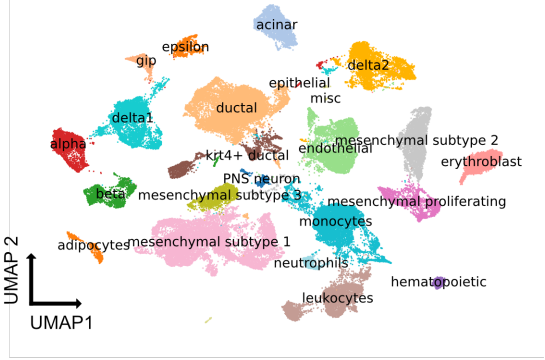

B

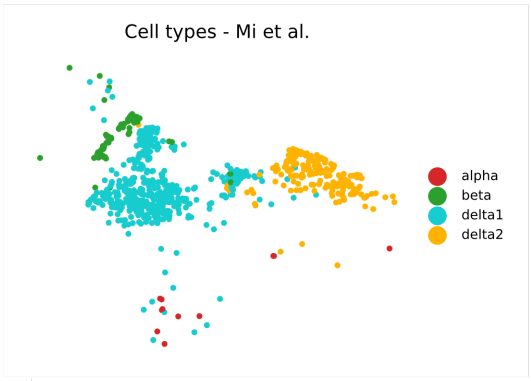

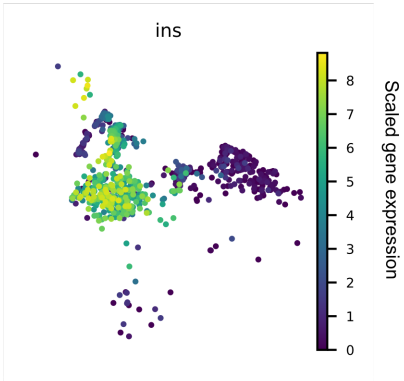

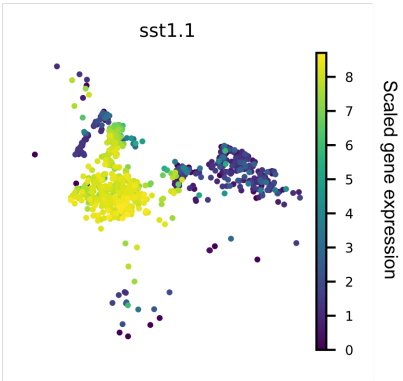

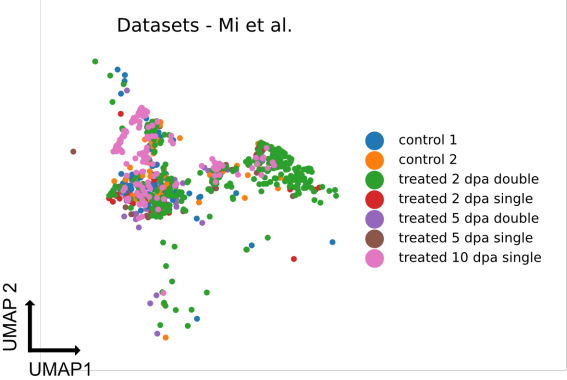

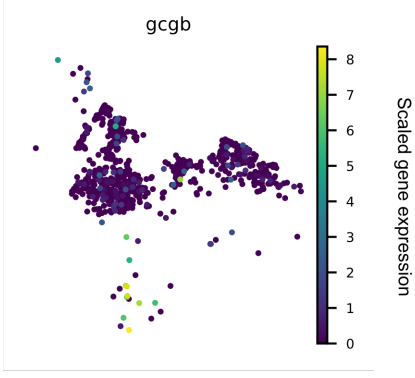

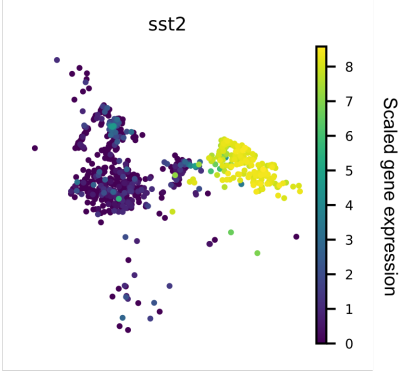

Supplementary Figure 1: A single-cell atlas of β-cell ablation shows that primed δ1 cells provide early insulin restoration across datasets

A) Cluster annotation of the integrated scRNA-sequencing dataset and utilized marker genes for annotation. All differential genes per cluster are listed in Supplementary Dataset S2**.**

B) Sub clustering of Figure 1D showing only data from Mi et al. 2023.

Supplementary Figure 2

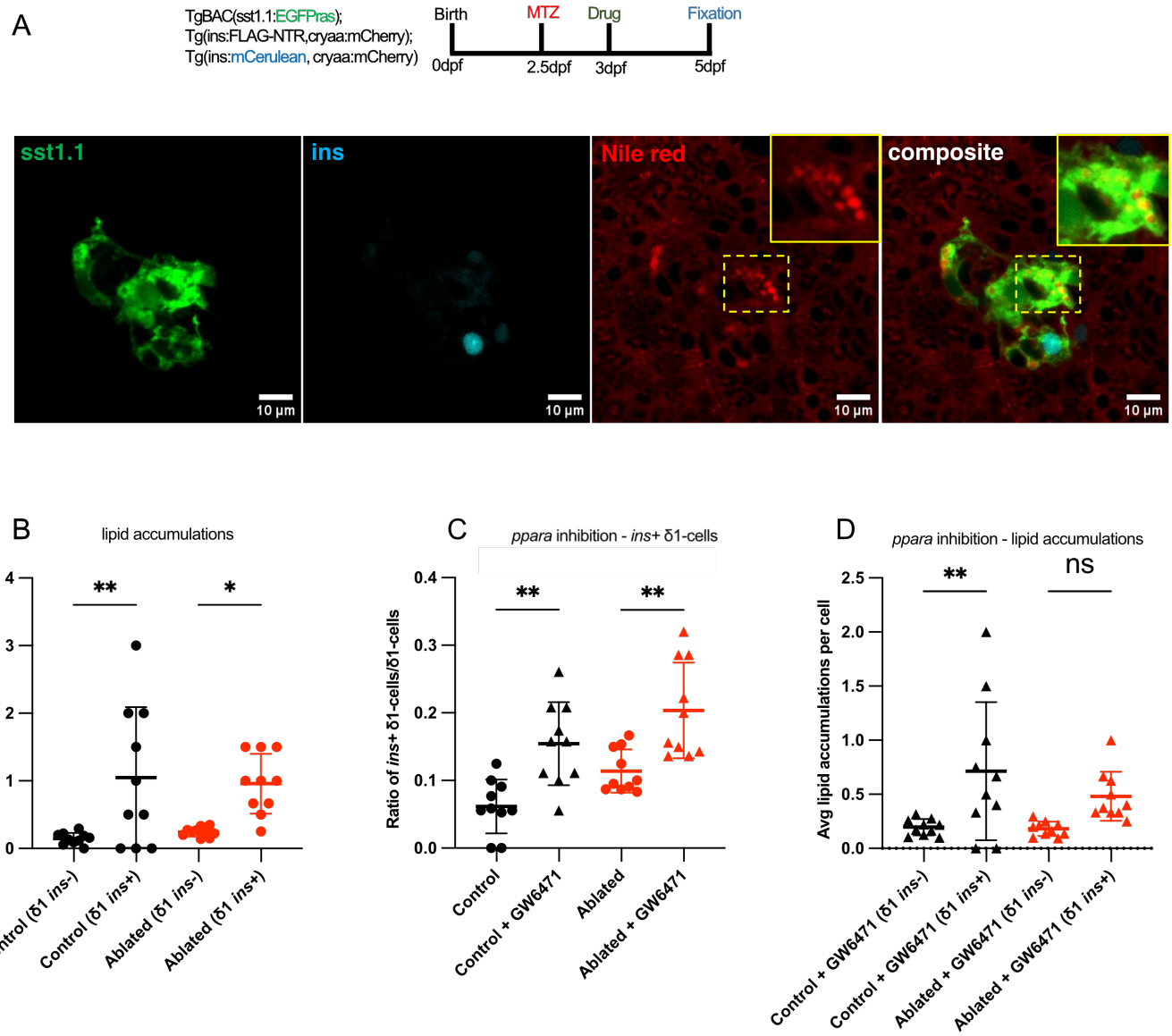

Supplementary Figure 2: Metabolic remodeling promotes *ins*$^{+}$ δ1-cell formation

A) Representative image of a larval pancreatic islet post β-cell ablation with lipid accumulations in δ1-cells. Lipids were stained using Nile Red. Scale bar: 10 μm.

B) Lipid accumulations are abundant in *ins*$^{+}$ δ1-cells but not in *ins*$^{-}$ δ1-cells, indicating altered lipid handling during the regenerative response. Each point represents one islet (n = 10 larvae). Statistical significance was determined using one-way ANOVA with Tukey's multiple comparisons test. Bars indicate mean ±1 SD.

C) Pharmacological inhibition of *PPARα* mediated fatty acid oxidation significantly increases the number of *ins*$^{+}$ δ1-cells, following β-cell ablation as well as in the unablated DMSO control. Larvae were treated with the PPARα antagonist GW6471. Each point represents one islet (n = 10 larvae). Statistical significance was determined using one-way ANOVA with Tukey's multiple comparisons test. Bars indicate mean ±1 SD.

D) Quantification of lipid accumulations in δ1-cells after treatment with the PPARα antagonist GW6471. Inhibition reduces the prevalence of lipid accumulations in *ins*$^{+}$ δ1-cells, in both treated and untreated larvae. Each point represents one islet (n = 10 larvae). Statistical significance was determined using one-way ANOVA with Tukey's multiple comparisons test. Bars indicate mean ±1 SD.

Supplementary Figure 3

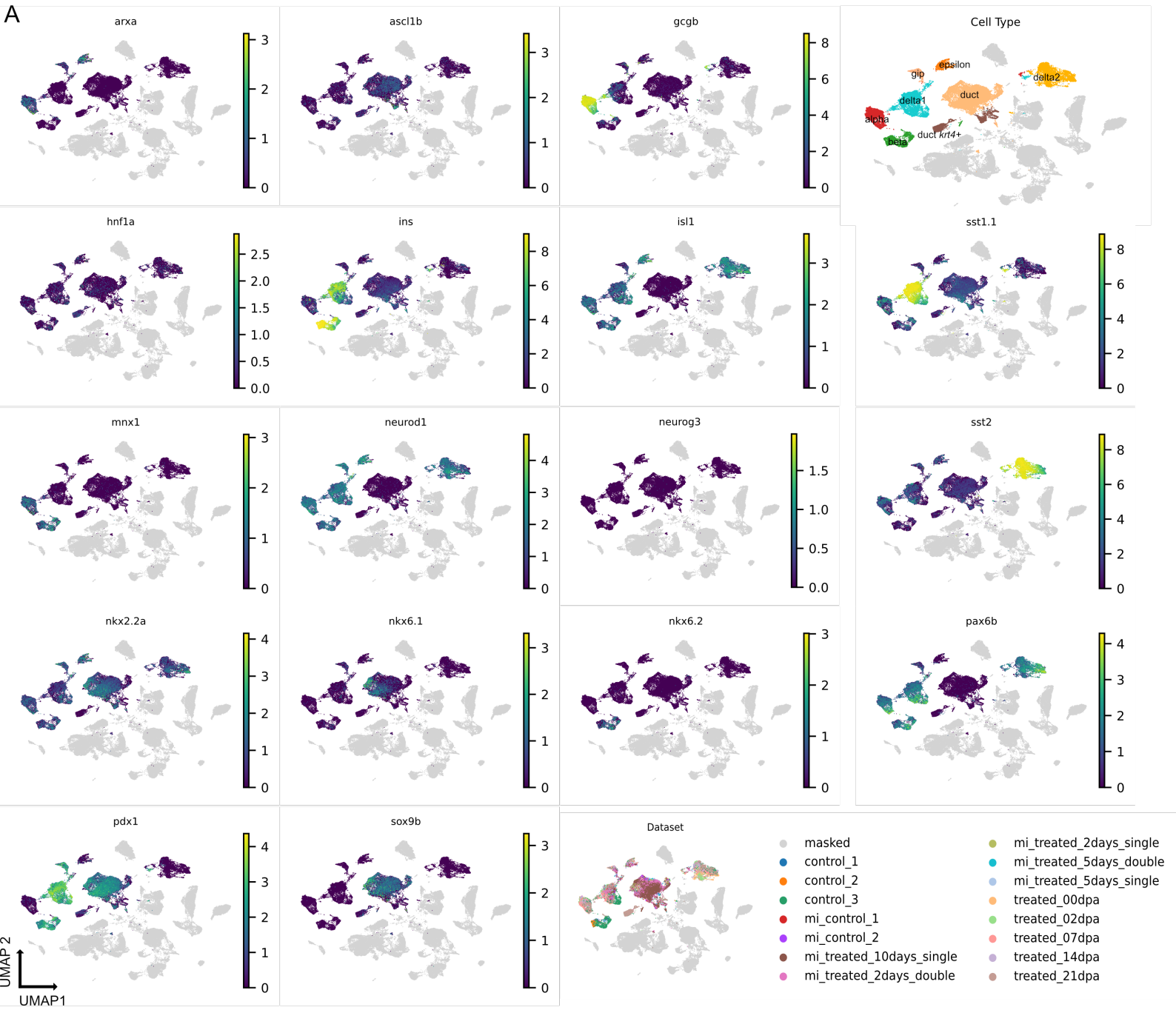

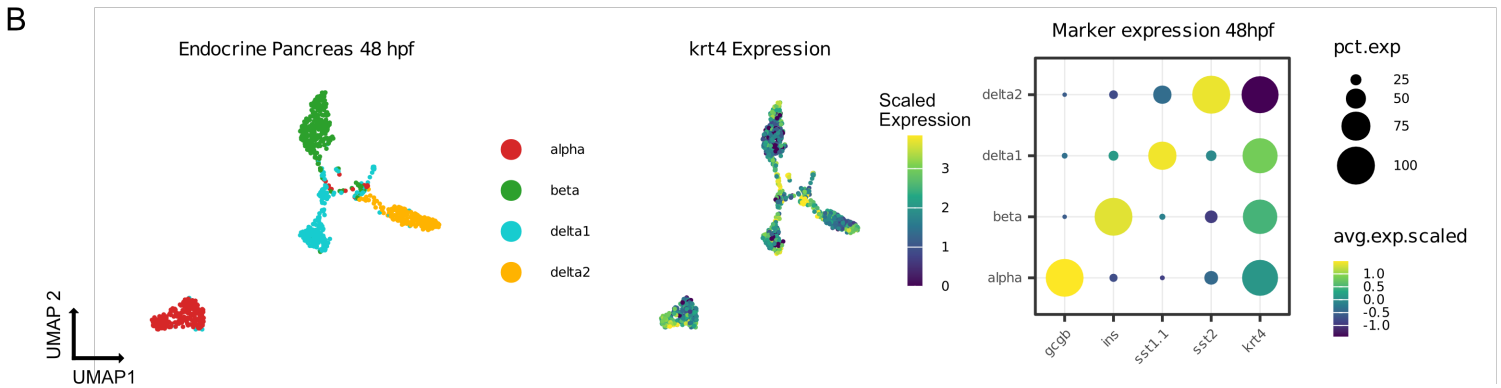

Supplementary Figure 3: Response of the pancreatic duct and origin of delta1 cells

A) Ductal cell populations do not express markers of endocrine progenitor cells post ablation. Marker genes derived from Prince et al. (Prince *et al*, 2017).

B) scRNA-seq data from zebrafish islets at 48 hpf show that endocrine cells are partially positive for expression of the ductal marker *krt4*.

Supplementary Figure 4

A

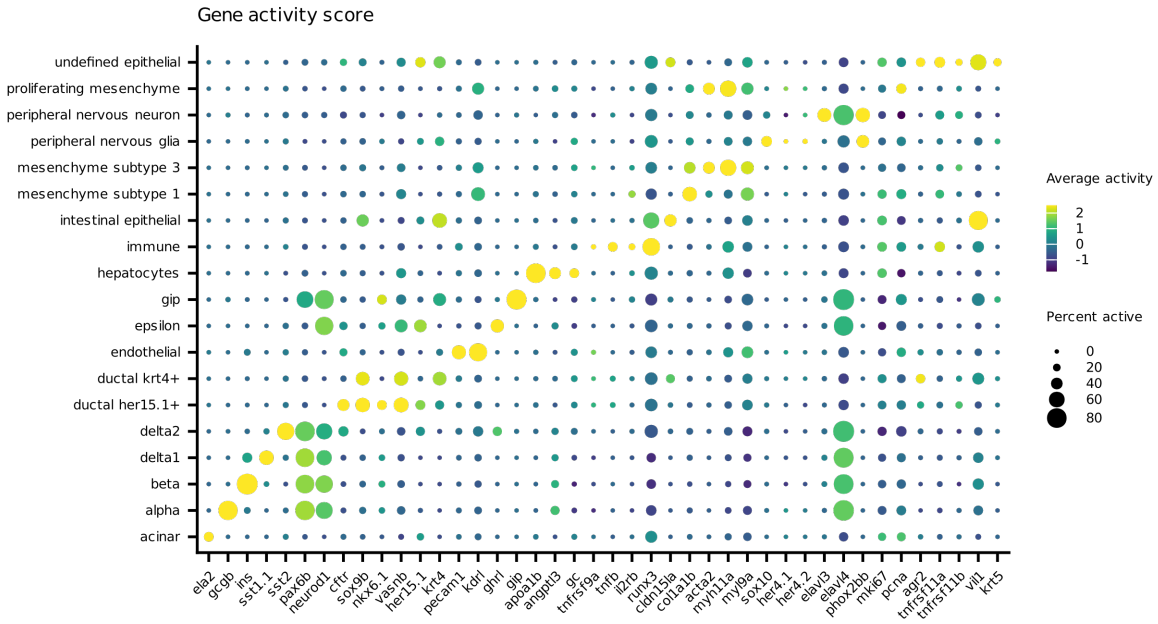

B

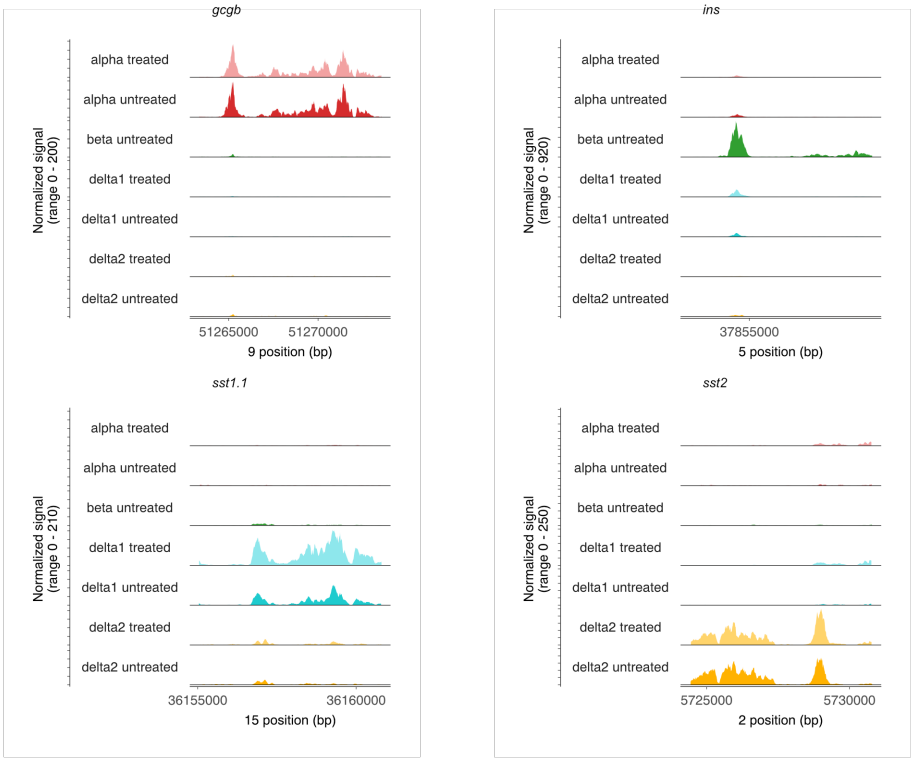

C

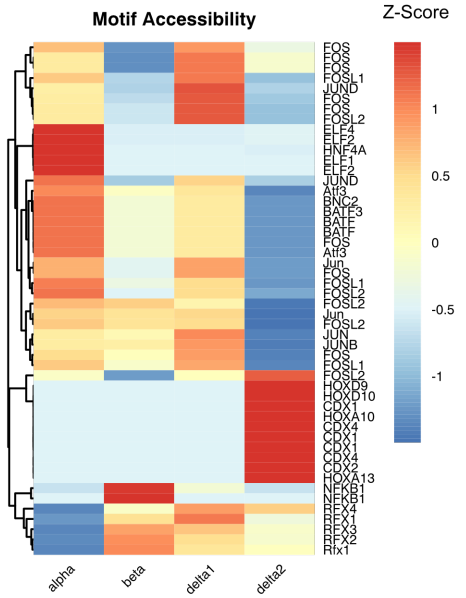

D

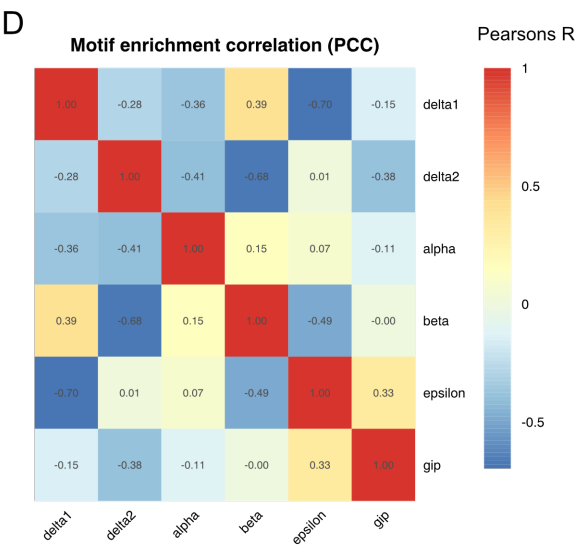

Supplementary Figure 4: Single cell ATAC sequencing data show chromatin accessibility landscape of the zebrafish pancreas

A) Marker gene activity used for annotation of zebrafish scATAC-seq data.

B) Chromatin accessibility plots of endocrine marker genes pre and post β-cell ablation.

C) Top motif accessibility by zebrafish cell type.

D) Pearson correlation coefficient of motif accessibility by cell type.

Supplementary Figure 5

A

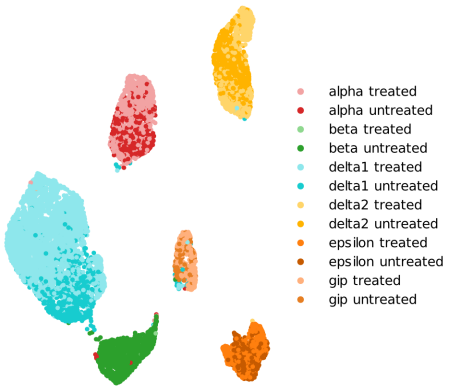

B

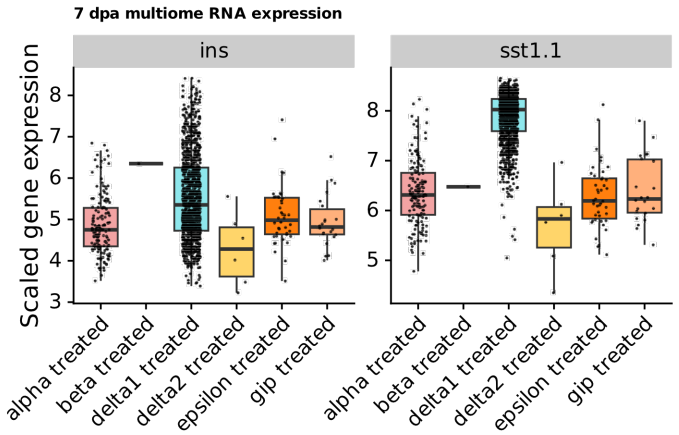

C

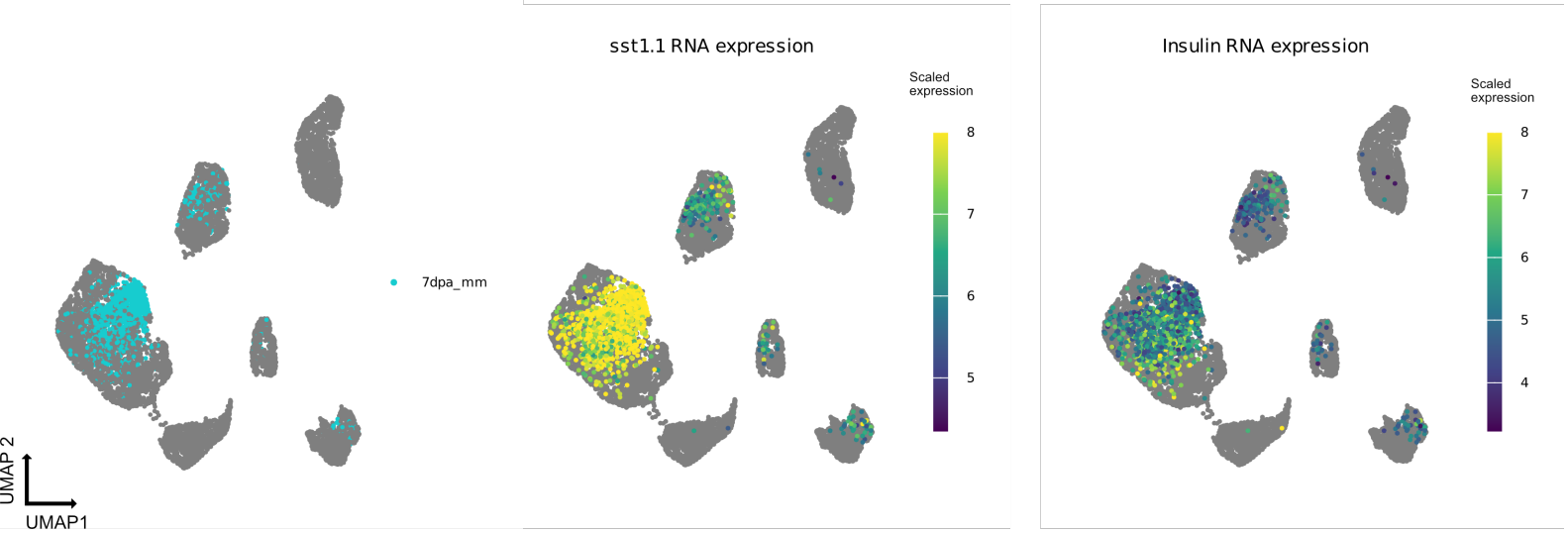

D

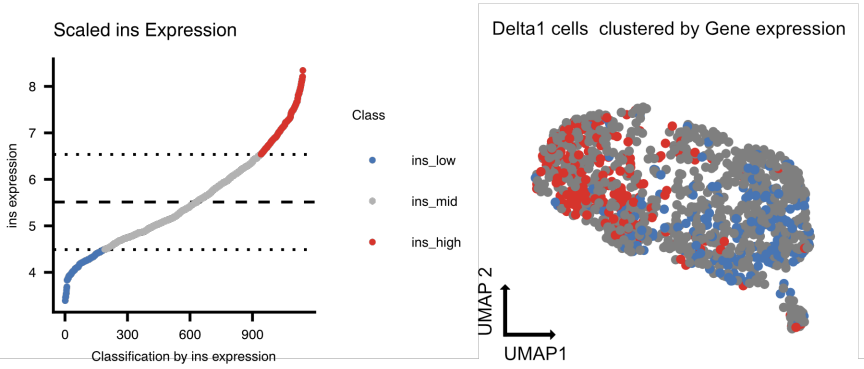

E

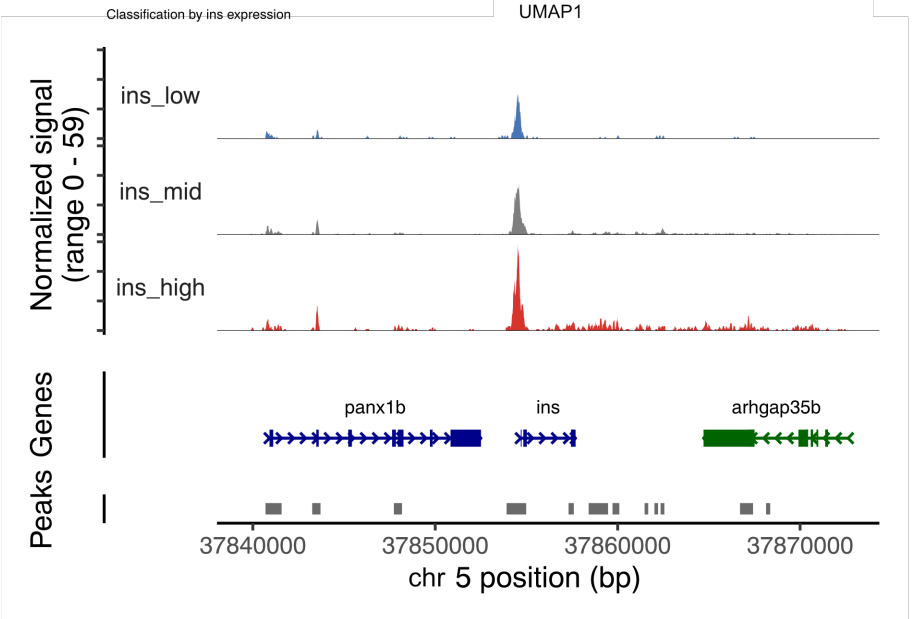

Supplementary Figure 5: Paired scRNA/scATAC-seq multiome data show δ1-cells express insulin without major chromatin remodeling

A) UMAP representation of scATAC-seq data of all endocrine cells (similar to Figure 2D).

B) Paired gene expression of *sst1.1* and *ins* in 7 dpa multiome data classified by scATAC-seq modality.

C) scATAC-seq data clustering does not separate ins^{+} and ins^{-} δ1-cells.

D) Classification of δ1-cells into ins_{high} and ins_{low} using the scRNA modality. Clustering of multiome δ1-cells by RNA modality allows separation between ins_{high} and ins_{low} δ1-cells.

E) Comparison of chromatin accessibility at the *ins* gene location between ins_{high} and ins_{low} δ1-cells.

Supplementary Figure 6

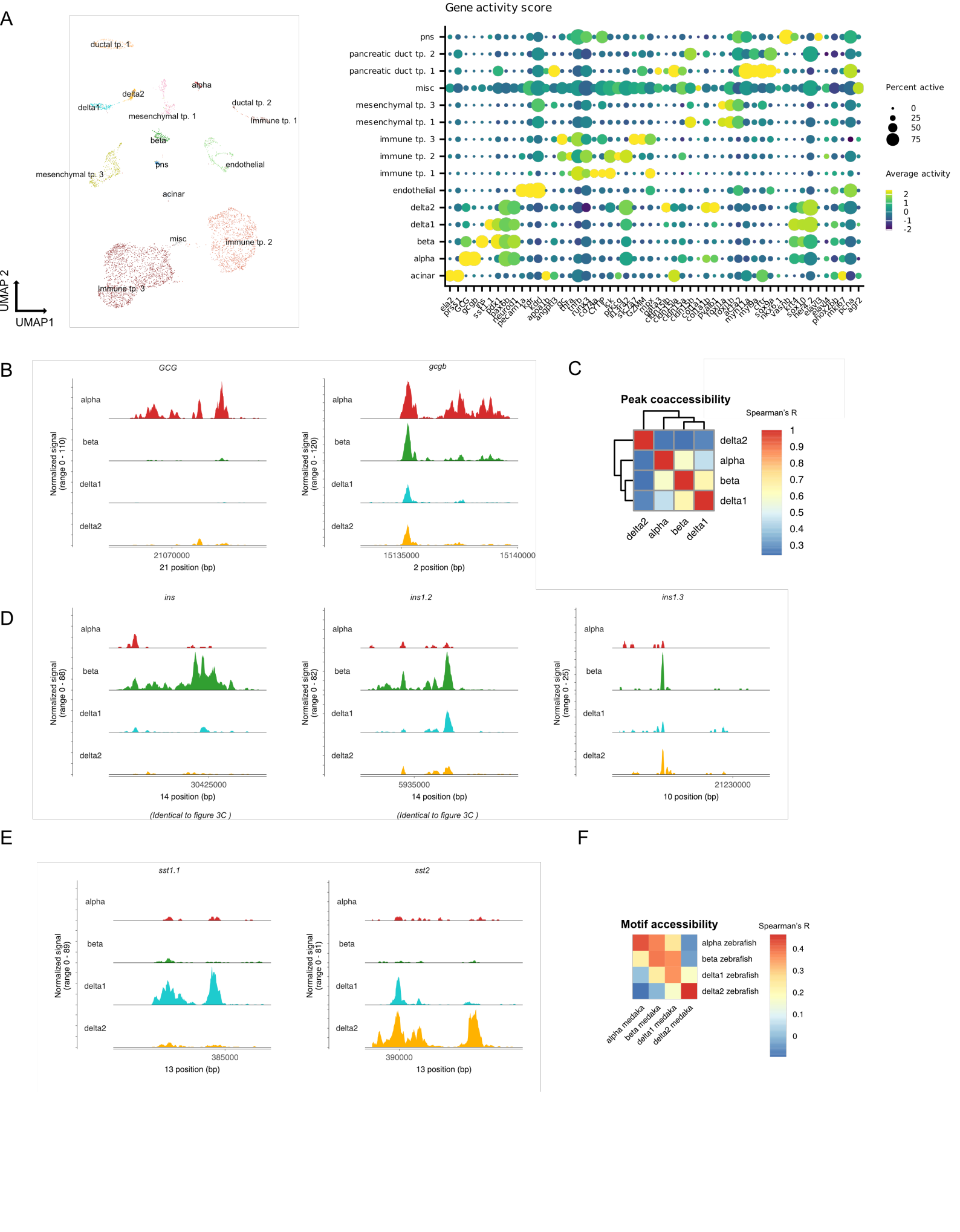

Supplementary Figure 6: Chromatin accessibility landscape of the medaka pancreas

A) Whole scATAC-seq dataset of medaka pancreas and surrounding tissues and gene accessibility used for cell type annotation. All differential accessible genes per cluster are listed in Supplementary Dataset S7**.**

B) Gene accessibility of α-cell markers *GCG* and *gcgb*.

C) Pearson correlation of peak co-accessibility in medaka islets.

D) Gene accessibility of medaka *ins* isoforms.

E) Gene accessibility of medaka *sst* isoforms.

F) Interspecies co-accessibility of motifs by cell type (Spearman’s correlation coefficient)

Supplementary Figure 7

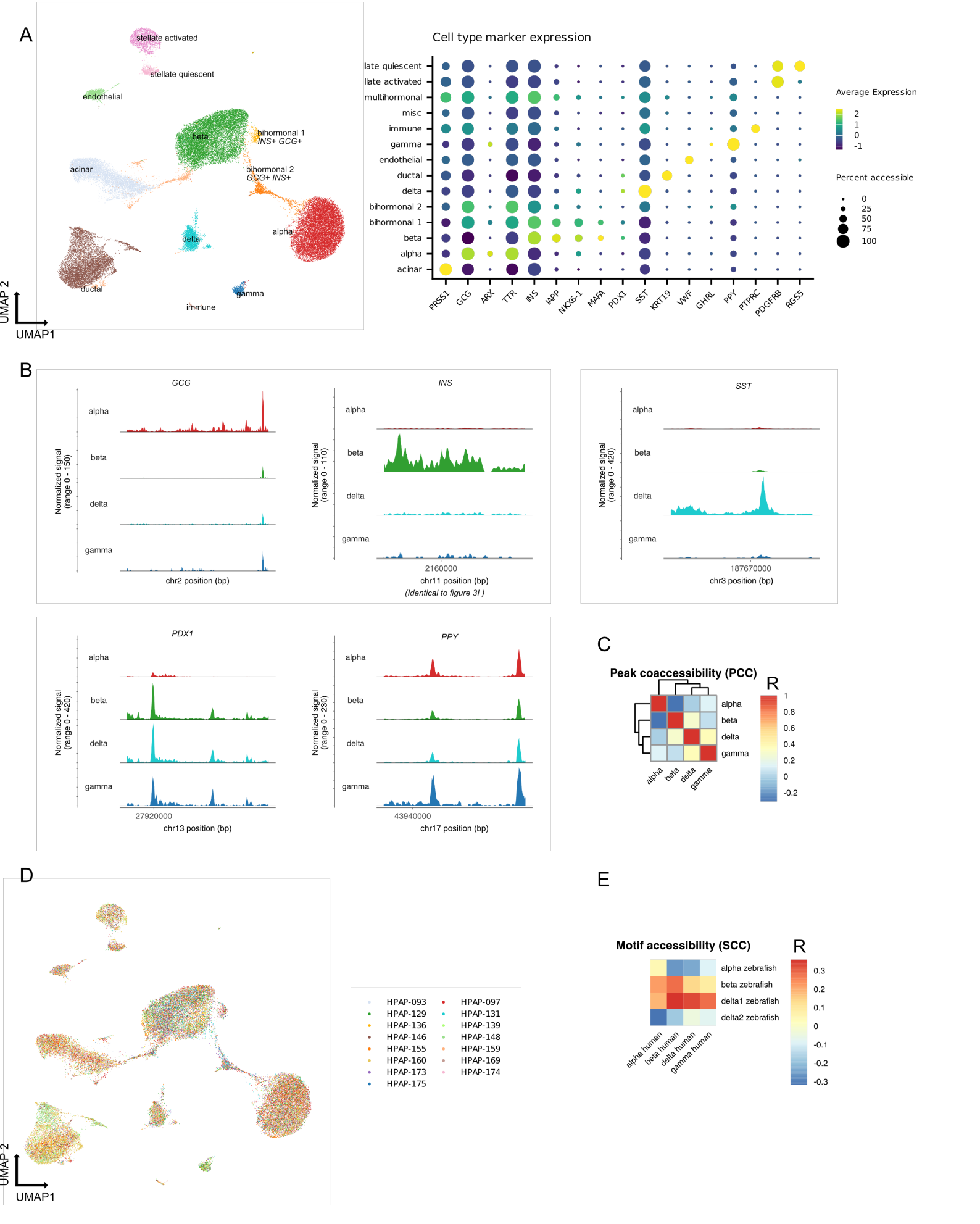

Supplementary Figure 7: Chromatin accessibility landscape of the healty human pancreas

A) UMAP representation and paired marker gene expression of multiome data from pancreata of 16 non-diabetic individuals as listed in Supplementary Dataset S1.

B) Chromatin accessibility by cell type of endocrine marker genes.

C) Pearson's correlation coefficient of peak co-accessibility.

D) Samples included in the dataset.

E) Interspecies coaccessibility of motifs by cell type (Spearman’s correlation coefficient)

Supplementary Figure 8

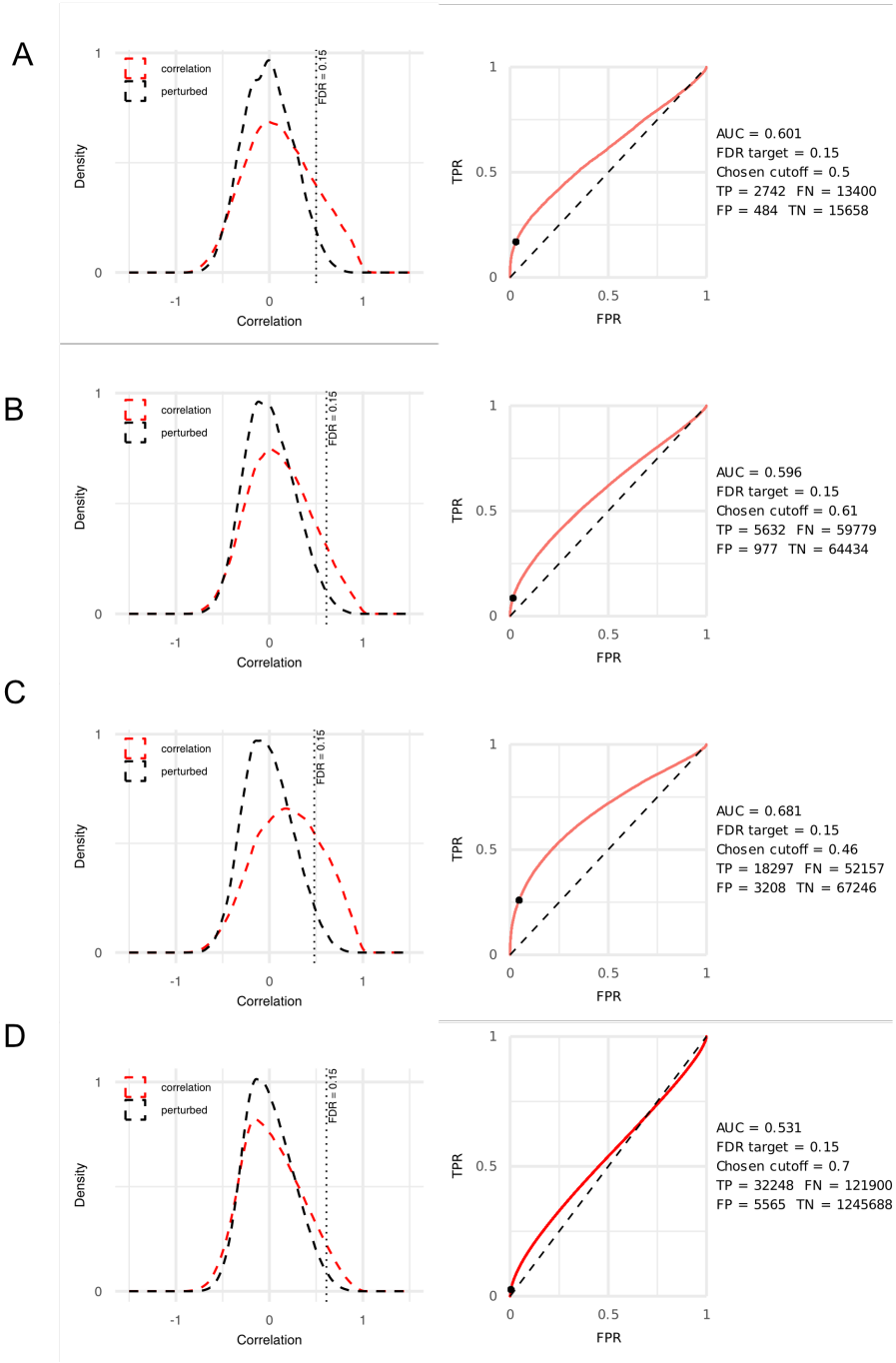

Supplementary Figure 8: Quality control and cutoff settings for GRN processing.

A) Pearson correlation of promoter (± 2kb) cCRE accessibility to target gene expression (red) vs random (black).

B) Pearson correlation of proximal (± 25kb) cCRE accessibility to target gene expression (red) vs random (black).

C) Pearson correlation of Sicero selected distal (± 500kb) cCRE accessibility to target gene expression (red) vs random (black).

D) Pearson correlation of transcription factor gene expression to putative target cCREs (red) vs random (black).

Supplementary Figure 9

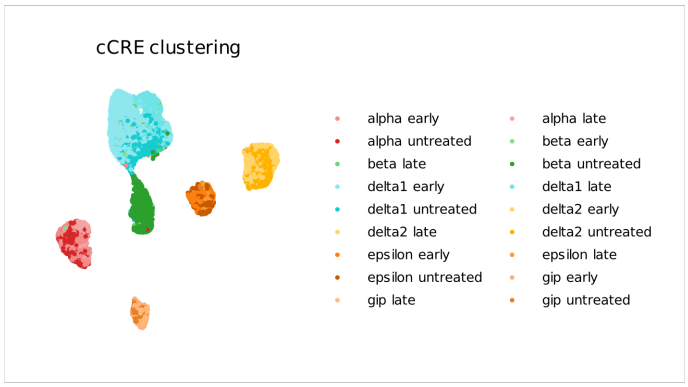

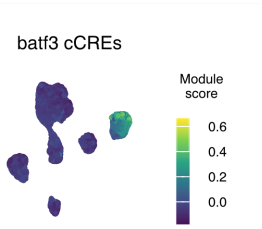

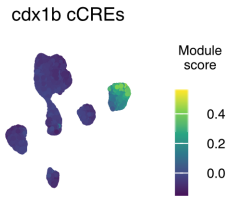

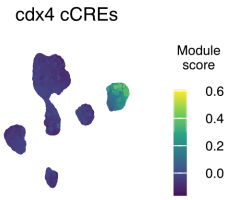

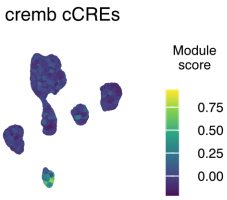

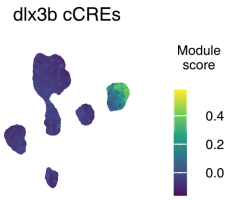

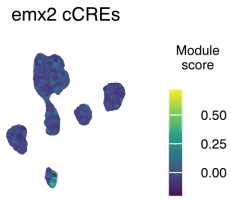

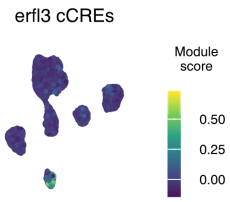

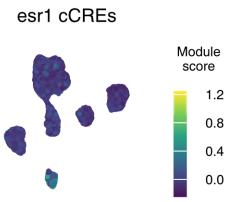

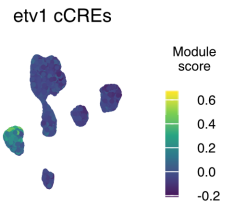

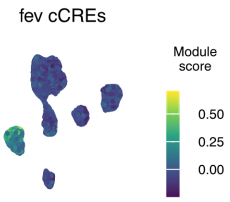

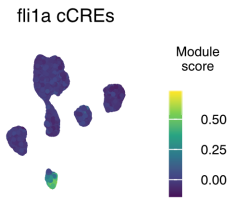

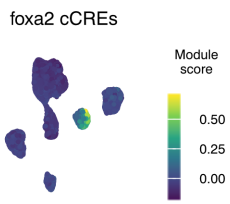

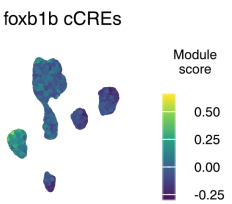

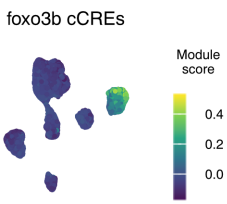

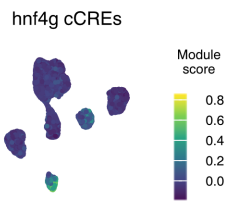

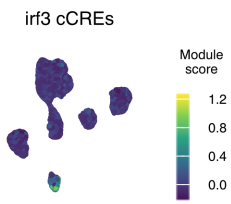

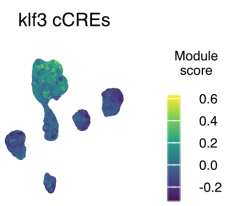

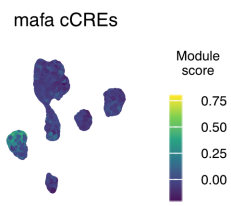

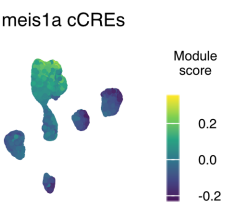

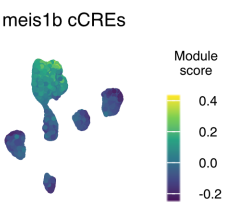

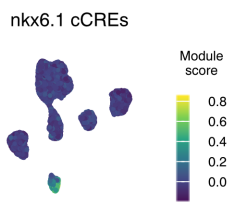

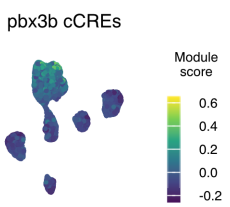

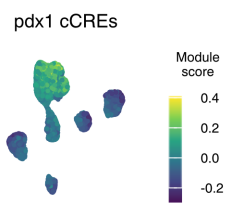

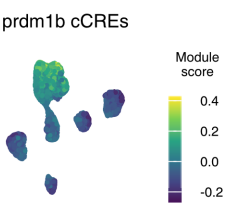

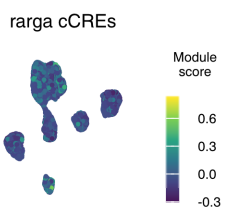

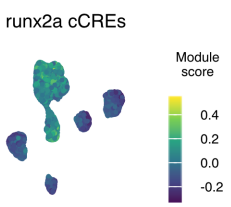

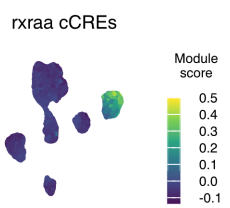

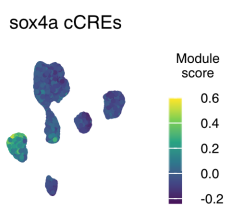

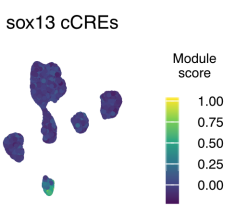

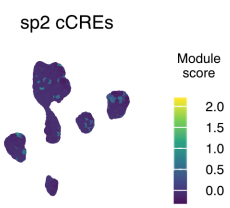

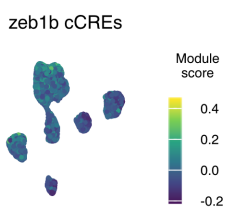

Supplementary Figure 9: TF module accessibility in endocrine cells

UMAP representation of endocrine cells using only cCREs which are linked to TF modules. Module accessibility scores represent the mean accessibility of all cCREs which are linked to a specific transcription factor, which allows identification of cell type specific programs.

Supplementary Figure 10

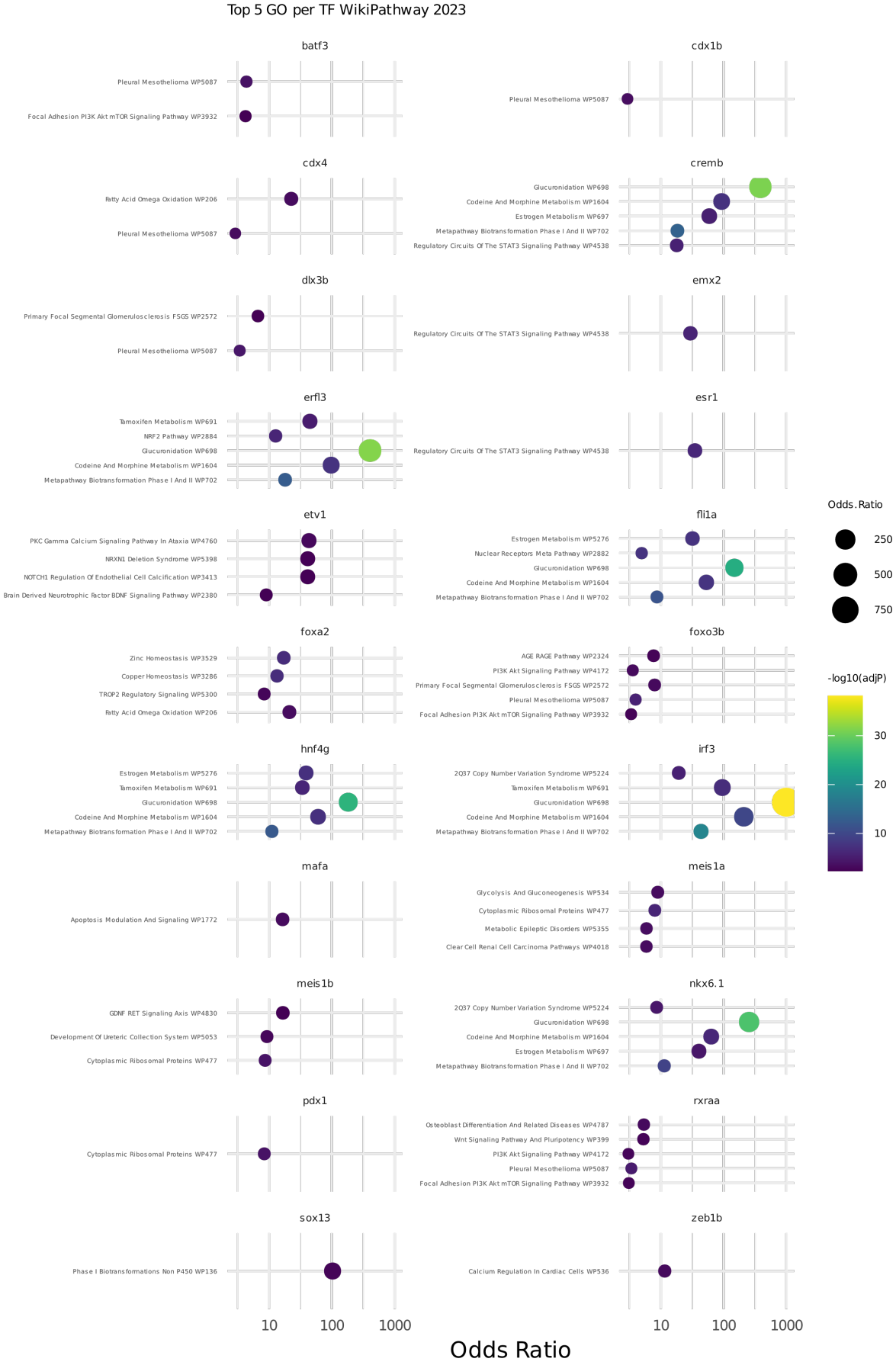

Supplementary Figure 10: Gene ontology enrichments terms of transcription factor target genes

Gene ontologies of differentially expressed genes post ablation linked to the respective transcription factors. Enrichment analysis was performed using enrichR with the WikiPathway database 2023.

Supplementary Figure 11

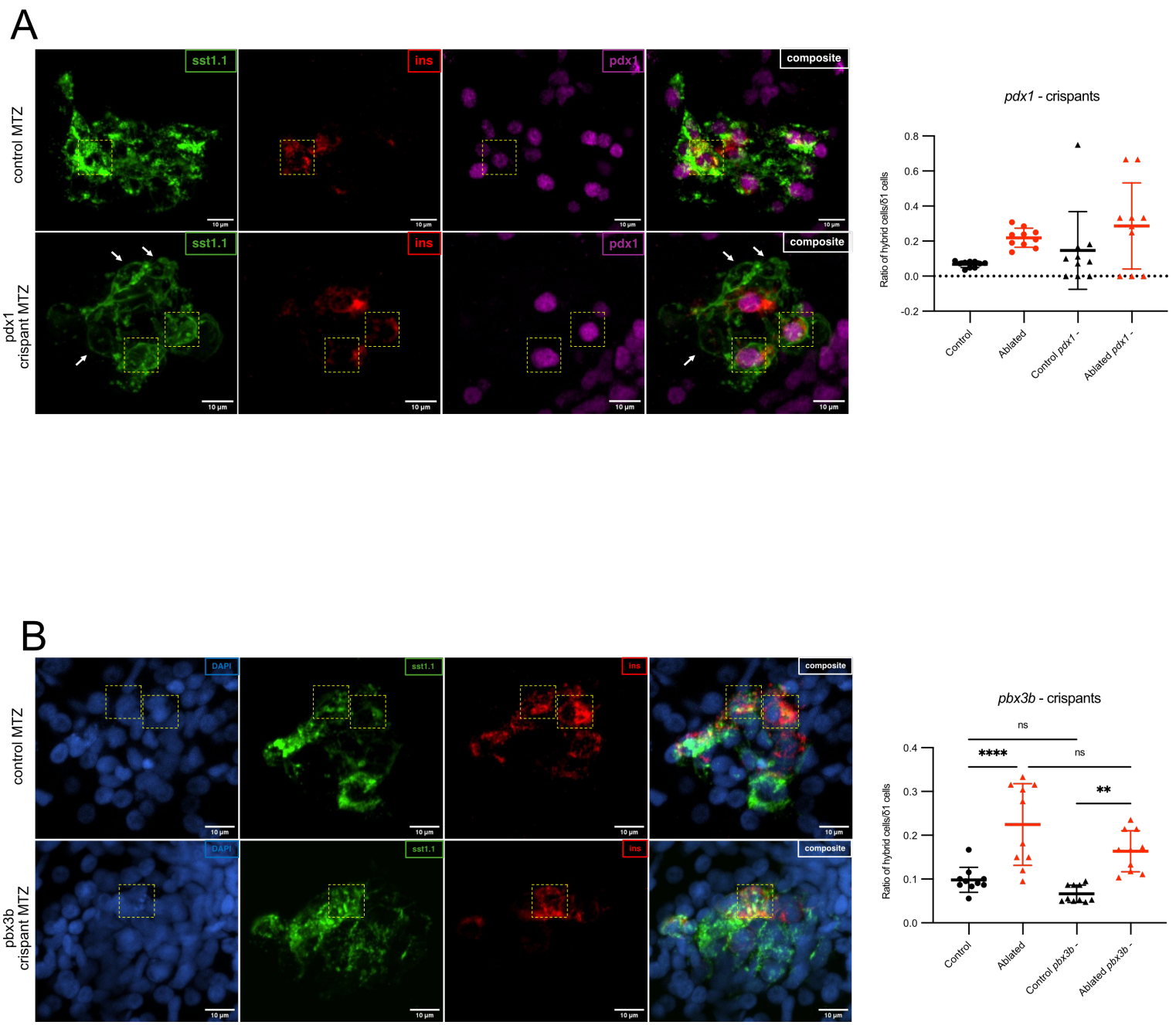

Supplementary Figure 11: Crispants of *pdx1* show disrupted islets while perturbations of *pbx3b* do not reduce numbers of hybrid cells

A) Representative confocal images and quantifications of hybrid cells in pancreatic islets after β-cell ablation and *pdx1* F0 knockouts. In control larvae, δ1-cells (*sst1.1*$^{+}$) activate insulin expression and form bihormonal hybrid cells. In F0 knockouts of *pdx1* targeting exon 2, islets are mostly disrupted. Antibody staining against insulin (red) and *pdx1* (magenta) show that existing hybrid cells are *pdx1* positive. White arrows indicate δ1-cells negative for pdx1 expression and yellow dotted squares indicate *sst1.1*$^{+}$/*ins*$^{+}$ double-positive cells.

B) Representative confocal images and quantifications of hybrid cells in pancreatic islets after β-cell ablation and *pbx3b* F0 knockouts with antibody staining against insulin (red). In control larvae, δ1-cells (*sst1.1*$^{+}$) activate insulin expression and form bihormonal hybrid cells. In F0 knockouts of *pbx3b*, the reduction of hybrid cells is not statistically significant. Yellow dotted squares indicate *sst1.1*$^{+}$/*ins*$^{+}$ double-positive cells.